frontiers | Frontiers in Physics

BRIEF RESEARCH REPORT
published: 27 April 2022
doi: 10.3389/fphy.2022.886962

Theoretical Investigation of Backward Optical Parametric Oscillator Pumped by Vortex Beams

Xiaosi Zhu, Jianlang He, Yawen Su, Yan Chen and Xiaopeng Hu**

National Laboratory of Solid State Microstructures, College of Engineering and Applied Sciences, School of Physics, Nanjing University, Nanjing, China

Nonlinear generation and manipulation of vortex beams have emerged as a research hot topic in recent years. During nonlinear frequency conversions, orbital angular momentum will transfer from the fundamental wave to harmonic waves. In this work, we study theoretically the backward optical parametric oscillator pumped by vortex beams. The orbital angular momentum conservation law has been disclosed for the counter propagation nonlinear process. In addition, the oscillation threshold and the conversion efficiency have been investigated in detail. Our results will be helpful for the experimental demonstration of backward optical parametric oscillator pumped by vortex beams.

Keywords: vortex beam, optical parametric oscillator, counter propagation nonlinear process, oscillation threshold, coupled-wave equation

OPEN ACCESS

Edited by:
Liangliang Lu,
Nanjing Normal University, China

Reviewed by:
Yan Sheng,
Australian National University, Australia
Lina Zhao,
Shandong Normal University, China

****Correspondence:***
Yan Chen
443928719@qq.com
Xiaopeng Hu
xphu@nju.edu.cn

Specialty section:
This article was submitted to Optics and Photonics, a section of the journal Frontiers in Physics

Received: *01 March 2022*
Accepted: *29 March 2022*
Published: *27 April 2022*

Citation:
Zhu X, He J, Su Y, Chen Y and Hu X (2022) Theoretical Investigation of Backward Optical Parametric Oscillator Pumped by Vortex Beams. Front. Phys. 10:886962. doi: 10.3389/fphy.2022.886962

INTRODUCTION

Light beams possessing an azimuthal phase front $e^{il\varphi}$ are called vortex beams [1], where $\varphi$is the azimuthal angle and l is an integer which indicates the topological charge of the optical vortex. Unlike the spin angular momentum of photons, which only has two possible states ± 1, theoretically achievable orbital angular momentum (OAM) states are infinite, that is, l is unbounded and can take any integer value. Vortex beams have unique characteristics such as a helical wave-front and a donut-shaped intensity profile. Such beams carry an OAM of $l\hbar$ per photon. Since l is unbounded, photons carrying OAM can carry multidimensional information. Due to the aforementioned characteristics of vortex beams, they have been extensively used in many applications, including super-resolution microscopy [2], optical tweezers [3, 4], and quantum information technology [5, 6]. The generation, manipulation, and detection of optical vortices are the focus of this research area. To generate vortex beams, the conventional ways are based on linear optics, such as vortex phase plate, spatial phase modulator based on computational holograph, and q-plate. However, these methods can only generate vortex beams with limited wavelength, since the devices usually have a limited operating wavelength bandwidth. In addition to the linear methods, nonlinear frequency conversion has been proved to be an important scheme to extend the operating wavelength of vortex beams [7–19]. For instance, the operating wavelength of vortex beams can be extended to the visible and ultraviolet band through frequency up-conversion processes such as third-harmonic generation (THG), sum-frequency generation (SFG), and high harmonic generation (HHG) [9–11]. In addition, vortex beams with tunable wavelength ranging from near-infrared to the mid-infrared can be obtained by parametric down-conversion processes such as difference-frequency generation (DFG) [12, 13] and optical parametric oscillation (OPO) [14–17]. Vortex beams in the mid-infrared region have the potential to be used in the areas of molecular spectroscopy and creating chiral nanostructures [20, 21]. For the OPOs pumped by vortex beams, the researchers reported that these are commonly in a

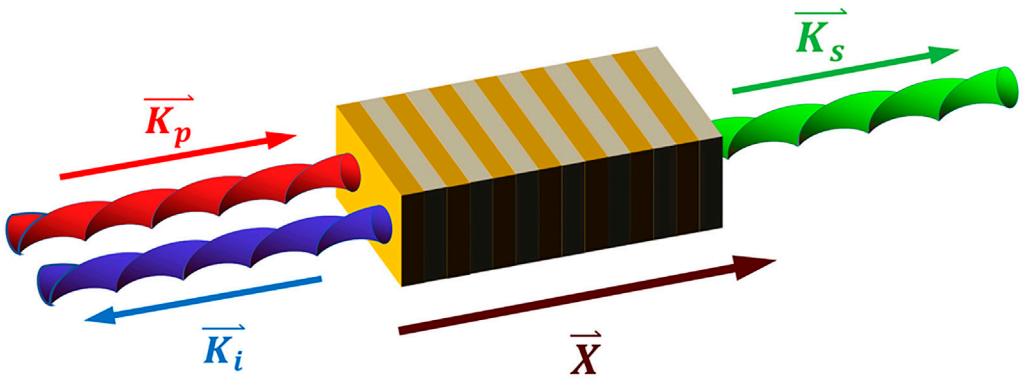

FIGURE 1 | Schematic of the backward OPO pumped by vortex beams.

forward-propagating configuration, which means the interacting waves are propagating in the same direction. As we know, in addition to the forward-propagating OPO, counter-propagating OPO [22, 23] is another type of configuration in which the interacting waves are propagating in the opposite directions. In backward OPO, the pump beam is down-converted into a counter-propagating signal and idler waves, and the oscillation is established by the distributed feedback due to the presence of two counter-propagating parametric waves. For the operation of backward OPOs, it does not require external mirrors or surface coating to form the optical cavity and operates in a simple single-pass geometry. Compared with conventional OPO, backward OPO has a simpler optical setup, a narrower linewidth, and less temperature sensitivity [24, 25]. Up to now, there is no research report on backward OPO pumped by vortex beams. In this work, we investigate in theory the backward OPO pumped by vortex beams using the nonlinear coupled-wave equations. The OAM conservation transfer law, the threshold, and the conversion efficiency of the vortex beam pumped backward OPO are studied.

THEORETICAL MODEL

Theoretically, the backward OPO pumped by vortex beams can be described by the coupled-wave equation. We assume that both the pump and the signal waves travel along the $+X$ direction, while the idler wave travels along the $-X$ direction. The polarization direction of the three beams is along the Z direction, corresponding to the Z axis of the KTP crystal, as shown in **Figure 1**.

The electric fields of the interacting waves are given by the following equation:

$$E_j = \sqrt{\frac{\omega_j}{n_j}} A_j u_j(\rho) e^{i(k_j z + l_j \varphi)\delta_j - i\omega_j t} + c.c\,, \tag{1}$$

where $j = p, i, s$ represents the pump, idler, and the signal wave, respectively. ρ and φ are the radius and azimuthal angle in the Z-Y plane, respectively. $\delta_j = 1$ *for* $j = p, s$, while $\delta_j = -1$ *for* $j = i$. ω_j, n_j, A_j, l_j, and u_j are the frequency, refractive index, amplitude, topological charge, and the normalized intensity profile of the three interacting waves, respectively. $k_j = 2\pi/\lambda_j$ is the wave vector of the corresponding light field, where λ_j is the wavelength. Substituting **Eq. 1** into the nonlinear coupled-wave equation [26] and considering the normalization condition $\int u^*_{p,s,i} u_{p,s,i} r dr d\varphi = 1$, we can obtain

$$\begin{aligned} \frac{dA_s}{dz} &= +i\kappa A_p A_i^* \exp(i\Delta k z), \\ \frac{dA_i}{dz} &= -i\kappa A_p A_s^* \exp(i\Delta k z), \\ \frac{dA_p}{dz} &= +i\kappa^* A_s A_i \exp(-i\Delta k z), \end{aligned} \tag{2}$$

where $\kappa = \frac{2}{c} d_{eff} S \sqrt{\frac{\omega_s \omega_i \omega_p}{n_s n_i n_p}}$ is the nonlinear coupling constant, with c being the velocity of light, d_{eff} being the effective nonlinear coefficient, and $S = \int u_s u_i u_p e^{i(l_p + l_i - l_s)} r dr d\varphi$ being the overlapping integral of the nonlinear process. $\Delta k = k_p + k_i - k_s$ is the wave vector mismatch of the backward OPO process. In order to achieve a high conversion efficiency of the counter-propagating nonlinear process, the quasi-phase-matching technique is desirable. Here in this work, we choose periodically poled KTP(PPKTP) as the quasi-phase-matched nonlinear crystal. For the KTP crystal, the difference of the lattice constant along the X and Y principal axes leads to the highly anisotropic domain growth velocity; thus, KTP is favorable for the fabrication of short-pitched periodically poled structures. Canaltas et al. demonstrated in an experiment the first backward OPO with a short-period PPKTP [27]. The first-order reciprocal vector provided by the PPKTP is $G = 2\pi/\Lambda$, with Λ being the poling period. Thus, the wave vector mismatch can be compensated by the reciprocal vector, that is, $\Delta k^{'} = \Delta k - G = 0$. At this time, **Eq. (2)** has the similar form as that under the plane wave approximation [28]. The difference is that the overlapping integral S between the interacting light fields should be considered in the nonlinear coupling constant of **Eq. (2)** in the backward OPO process involved with vortex light. In order to ensure that the overlapping integral is non-zero, the topological charges of

the pump, signal, and idler waves should satisfy the following relationship:

$$l_p = l_s - l_i\,. \tag{3}$$

Equation 3 is the OAM conservation condition in the backward OPO, which is different from that in conventional OPO due to the reversed propagation direction of the idler wave.

Equation 3 presents the OAM conservation law of the backward OPO, and in principle, there are infinite combinations of the topological charge of the signal and idler waves [l_s, l_i] satisfying the OAM conservation. To determine the OAM transfer in an optical parametric oscillator, one should consider the threshold of each combination, which is the basic knowledge of mode selection in the laser techniques. In previous studies, OAM transfer in the OPO process can be controlled by adjusting the cavity losses or the spatial overlap integral of the interaction waves [29–31]. The purpose is to change the OPO threshold of different combinations since the OAM preferentially transfers to the combination with the lower threshold. Therefore, we use the method in Ref. [28] to solve **Eq. 2** to obtain the threshold of the backward OPO pumped by vortex beams:

$$P_{th} = \frac{c\varepsilon_0 n_s n_i n_p \lambda_s \lambda_i}{32 L^2 d_{eff}^2 S^2}, \tag{4}$$

where ε_0 is the permittivity of vacuum and L is the nonlinear interaction length. The Rayleigh distance of light waves is set to be much longer than the sample length, thus the overlapping integral is approximately constant and equal to that in the beam waist.

According to **Eq. 4**, the threshold P_{th} for the backward OPO is inversely proportional to the square of overlapping integral. When the topological charge of [l_s, l_i] the pump wave is fixed, processes with different combinations correspond to different overlapping integrals. Therefore, in order to control the OAM conversion and ensure the purity of output beams, we can control the pump power to only excite the process with the largest overlap integral.

In the study, we assume that the pump, signal light, and idler light are in the form of the Laguerre–Gaussian mode [1], and have the same confocal parameters [32]:

$$\frac{n_p w_p^2}{\lambda_p} = \frac{n_s w_s^2}{\lambda_s} = \frac{n_i w_i^2}{\lambda_i}, \tag{5}$$

where w_p, w_s, w_i are the beam waist radius of the three interacting waves, respectively. By substituting the normalized light intensity of a Laguerre–Gaussian mode, the OAM conservation law $|l_p| = |l_s| + |l_i|$, and **Eq. 5** into the expression of the overlapping integral, the overlapping integral of light field at the beam waist is as follows:

$$S_{l_p,l_s,l_i} = \sqrt{\frac{2}{\pi}} \cdot \sqrt{\frac{|l_p|!}{|l_s|! \cdot |l_i|!}} \cdot \frac{\gamma_s^{|l_s|+1} \gamma_i^{|l_i|+1}}{w_p} \times \left(\frac{2}{1+\gamma_s^2+\gamma_i^2}\right)^{|l_p|+1}, \tag{6}$$

where $\gamma_s = w_p/w_s$, $\gamma_i = w_p/w_i$. We should be aware that the combination with $|l_p| = |l_s| - |l_i|$ may also satisfy the OAM conservation condition, but the overlapping integral of the corresponding process is smaller than that with $|l_p| = |l_s| + |l_i|$, and thus the discussions are not included in this article.

RESULTS AND DISCUSSIONS

When OAM conservation in **Eq. 3** is satisfied, we use **Eq. 6** to calculate the overlapping integrals of all the combinations of l_s and l_i when the pump light carries three different OAMs, as shown in **Figure 2**. For the numerical calculations, the temperature was set at 100°C, the beam waist was set to be $w_p = 150\ \mu m$, and the pump light wavelength was 1.064 μm. We systematically studied the backward OPO process when the wavelength of signal wave is in the range of 1.5 – 2.128 μm.

As shown in **Figure 2A**, when the signal wavelength of the output signal is near the degenerate point, the overlapping integral of $S_{1,0,-1}$ and $S_{1,1,0}$ is close; hence, both processes may oscillate. As the signal wavelength decreased from the degeneracy point, the $S_{1,1,0}$ increases while the $S_{1,0,-1}$ decreases gradually, which means $S_{1,1,0}$ is more preferentially to oscillate than $S_{1,0,-1}$. Thus, the OAM of the pump wave tends to transfer to the signal wave. **Figures 2B,C** have the same trends. When the signal light wavelength is in the range of 1.7–1.9 μm, $S_{1,1,0}$, $S_{2,1,-1}$, and $S_{3,2,-1}$ are obviously larger than the other [l_s, l_i] combinations when l_P is 1,2, and 3, respectively. From **Figure 2C**, we can see that the overlap integral of $S_{3,1,-2}$ and $S_{3,-1,2}$ is higher than that of $S_{3,0,-3}$ and $S_{3,3,0}$, and this can be explained as follows. At the degenerated point, the beam waist of the signal and the idler waves are the same. For $S_{3,1,-2}$ and $S_{3,-1,2}$, the signal and the idler waves are both vortex beams, while for $S_{3,0,-3}$ and $S_{3,3,0}$, the parametric waves, respectively, possess a Gaussian profile and a vortex one. According to the calculation, the overlap integral between the two vortex beams is larger than that between a Gaussian beam and a vortex beam; hence, the overlap integral for $S_{3,1,-2}$ and $S_{3,-1,2}$ is larger than the situation for $S_{3,0,-3}$ and $S_{3,3,0}$. Next, we will make a detailed analysis of the threshold of the backward OPO when the wavelength of the signal wave is set to be $\lambda_s = 1.8\ \mu m$. **Eq. 4** is used to obtain the relationship between the OPO threshold and the sample length when the topological charge of the pump wave is $l_p = 3$, and the relationship is plotted in **Figure 3A**.

As can be seen from **Figure 3A**, the oscillation threshold decreases with the increase in the length of the nonlinear crystal. Meanwhile, the difference in the threshold value among the different [l_s, l_i] combinations becomes smaller. The results imply that the threshold difference between different combinations [l_s, l_i] of the backward OPOs can be controlled by varying the length of the nonlinear crystal. **Figure 3B** shows the pump threshold of the processes with the largest overlap integrals with different interaction lengths and different topological charges of the pump wave, which follows the same trend as that in **Figure 3A**. Moreover, the oscillation threshold increases with the increase in the topological charges of the pump. In **Figure 3B**, we list the threshold of the combination [l_s, l_i] when $l_p = 0, 1, 2, 3$, respectively, and then we can control the pump power for more precise excitation of the required backward OPO.

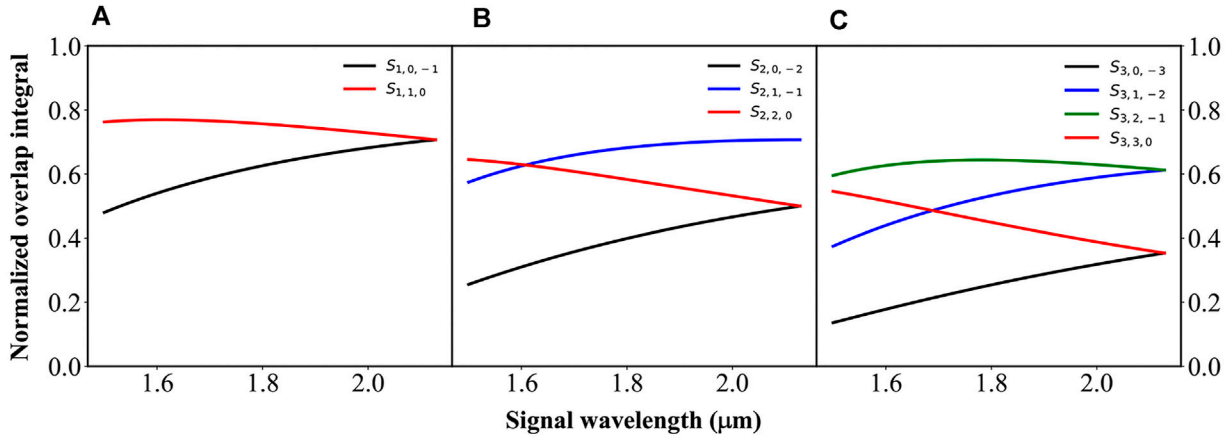

FIGURE 2 | Overlapping integral of different combinations [l_s, l_i], which is normalized by set $S_{0,0,0}$ to be 1 at the degeneracy point. The topological charge of the pump wave is **(A)** $l_p = 1$, **(B)** $l_p = 2$, and **(C)** $l_p = 3$.

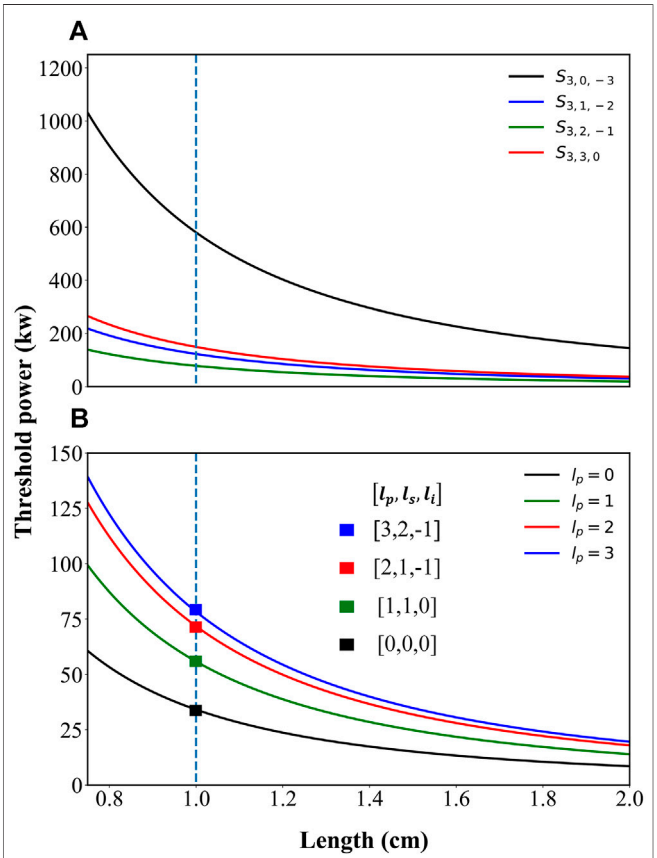

FIGURE 3 | Relationship between the OPO threshold and the sample length. **(A)** Situations for all [l_s, l_i] combinations when the topological charge of the pump wave is set to be $l_p = 3$. **(B)** Situations in which the [l_s, l_i] combination takes the largest overlap integral with different topological charge of the pump wave.

The conversion efficiency η is a key parameter, and under a stable oscillation state, it is determined by the following formula, which can be obtained by solving **Eq. 2**:

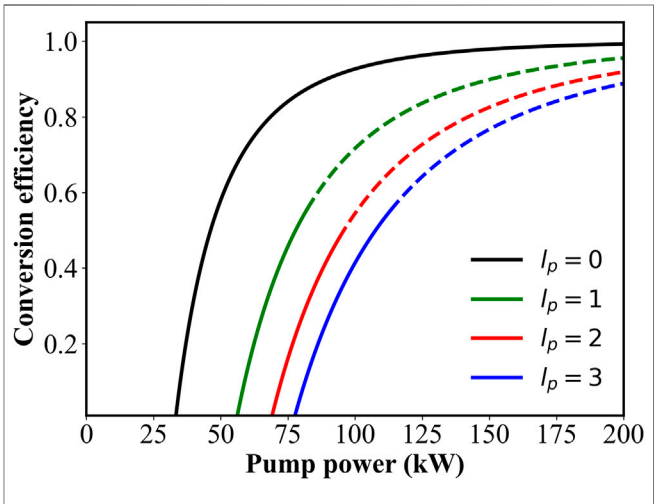

FIGURE 4 | Relationship of the conversion efficiency varying with the pump power. The solid lines represent the single mode excitation (the lowest oscillation threshold is reached), and the dotted lines represent the multiple mode excitation.

$$\int_0^{\frac{\pi}{2}} \frac{d\theta}{\sqrt{1-\eta sin^2\theta}} = \frac{\pi}{2} \cdot \sqrt{\frac{P_p}{P_{th}}}, \tag{7}$$

where P_p is the power of the pump wave and θ is the incident angle of the pump wave [28]. Here, we assume that the length of PPKTP is 1 cm, and the relationship between the conversion efficiency and the peak power of the pump wave with different topological charge of the pump wave is shown in **Figure 4**.

According to **Figure 4**, we can see that when the input power of the pump light exceeds the threshold, the conversion efficiency increases rapidly. Since only the [l_s, l_i] combination with the largest overlapping integral is considered in the calculation of **Eq. 7**, and when the pump power is too high, processes with a high threshold may also oscillate. Thus, the purity of the output vortex

light will be reduced, and the efficiency curve may not be accurate (dotted lines). In the experiment, it would be better if we controlled the input power in the solid line area; thus, we can ensure a high purity OAM state of the signal wave.

For practical realization of the backward OPO pumped by vortex beams, a high-energy pulsed laser light source together with a sub-micrometer periodically poled KTP is required. In our theoretical investigations, we choose a long-pulsed laser as the pump rather than ultrashort pulses because oscillation may not be observed due to the appearance of stimulated Raman scattering at pulses shorter than 20 pico-seconds [27]. The main difficulty of the practical demonstration is the nonlinear crystal. For backward OPO, a sub-micrometer QPM structure is required; however, fabrication of such a structure is still a big challenge. Up to now, there are only a few reports on the experimental demonstration of backward OPOs with Gaussian beams as the pump.

CONCLUSION

In this study, we have investigated the backward OPO pumped by vortex beams using the nonlinear coupled-wave equations. The OAM conservation law was determined to be $l_p = l_s - l_i$, which is different from that of the conventional forward-propagating OPO. To figure out the OAM transfer during the backward OPO process, we studied the oscillation threshold for different topological charge combinations of the signal and the idler waves, which is closely related to the overlapping integral, the length of the nonlinear crystal, and the topological charge of the pump wave. In addition, the conversion efficiency of the oscillation was numerically calculated. Our results can help understand the OAM transfer in the backward OPO, and obtain the output vortex beam with a pure OAM component. Further work will be focused on the experimental demonstration of the backward OPO pumped by vortex beams.

DATA AVAILABILITY STATEMENT

The raw data supporting the conclusions of this article will be made available by the authors, without undue reservation.

AUTHOR CONTRIBUTIONS

XH and YC proposed the idea. XZ, JH, and YS performed the theoretical analysis and numerical simulations. XZ, YC, and XH wrote the manuscript with contributions from all co-authors.

FUNDING

This work was supported by the National Key R&D Program of China (Nos. 2019YFA0705000 and 2017YFA0303700), the National Natural Science Foundation of China (Nos. 12174185, 91950206, 92163216, and 51890861), the Leading-edge Technology Program of Jiangsu Natural Science Foundation (No. BK20192001), and the Key R&D Program of Guangdong Province (No. 2018B030329001).

REFERENCES

1. Allen L, Beijersbergen MW, Spreeuw RJC, Woerdman JP. Orbital Angular Momentum of Light and the Transformation of Laguerre-Gaussian Laser Modes. *Phys Rev A* (1992) 45(11):8185–9. doi:10.1103/PhysRevA.45.8185
2. Harke B, Keller J, Ullal CK, Westphal V, Schönle A, Hell SW. Resolution Scaling in STED Microscopy. *Opt Express* (2008) 16(6):4154–62. doi:10.1364/OE.16.004154
3. Gahagan KT, Swartzlander GA. Optical Vortex Trapping of Particles. *Opt Lett* (1996) 21(11):827–9. doi:10.1364/OL.21.000827
4. Grier DG. A Revolution in Optical Manipulation. *Nature* (2003) 424(6950):810–6. doi:10.1038/nature01935
5. Trichili A, Rosales-Guzmán C, Dudley A, Ndagano B, Ben Salem A, Zghal M, et al. Optical Communication beyond Orbital Angular Momentum. *Sci Rep* (2016) 6(1):27674. doi:10.1038/srep27674
6. Willner AE, Huang H, Yan Y, Ren Y, Ahmed N, Xie G, et al. Optical Communications Using Orbital Angular Momentum Beams. *Adv Opt Photon* (2015) 7(1):66–106. doi:10.1364/AOP.7.000066
7. Hu X, Zhang Y, Zhu S. Nonlinear Beam Shaping in Domain Engineered Ferroelectric Crystals. *Adv Mater* (2020) 32(27):1903775. doi:10.1002/adma.201903775
8. Chen Y, Ni R, Wu Y, Du L, Hu X, Wei D, et al. Phase-Matching Controlled Orbital Angular Momentum Conversion in Periodically Poled Crystals. *Phys Rev Lett* (2020) 125(14):143901. doi:10.1103/PhysRevLett.125.143901
9. Xu Z, Lin Z, Ye Z, Chen Y, Hu X, Wu Y, et al. Control the Orbital Angular Momentum in Third-Harmonic Generation Using Quasi-Phase-Matching. *Opt Express* (2018) 26(13):17563–70. doi:10.1364/OE.26.017563
10. Li Y, Zhou Z-Y, Ding D-S, Shi B-S. Sum Frequency Generation with Two Orbital Angular Momentum Carrying Laser Beams. *J Opt Soc Am B* (2015) 32(3):407–11. doi:10.1364/JOSAB.32.000407
11. Gauthier D, Ribič PR, Adhikary G, Camper A, Chappuis C, Cucini R, et al. Tunable Orbital Angular Momentum in High-Harmonic Generation. *Nat Commun* (2017) 8(1):14971. doi:10.1038/ncomms14971
12. Huguenin JAO, Martinelli M, Caetano DP, santos BCd., Almeida MP, Ribeiro PHS, et al. Orbital Angular Momentum Exchange in Parametric Down Conversion. *J Mod Opt* (2006) 53(5-6):647–58. doi:10.1080/09500340500217548
13. Arlt J, Dholakia K, Allen L, Padgett MJ. Parametric Down-Conversion for Light Beams Possessing Orbital Angular Momentum. *Phys Rev A* (1999) 59(5):3950–2. doi:10.1103/PhysRevA.59.3950
14. Smith A, Armstrong D. Generation of Vortex Beams by an Image-Rotating Optical Parametric Oscillator. *Opt Express* (2003) 11(8):868–73. doi:10.1364/OE.11.000868
15. Horikawa M-T, Ogawa A, Miyamoto K, Yusufu T, Omatsu T. Handedness Control in a Tunable Midinfrared (60-125 μm) Vortex Laser. *J Opt Soc Am B* (2015) 32(12):2406–10. doi:10.1364/JOSAB.32.002406
16. Yusufu T, Tokizane Y, Yamada M, Miyamoto K, Omatsu T. Tunable 2-μm Optical Vortex Parametric Oscillator. *Opt Express* (2012) 20(21):23666–75. doi:10.1364/OE.20.023666
17. Furuki K, Horikawa M-T, Ogawa A, Miyamoto K, Omatsu T. Tunable Mid-infrared (63-12 μm)optical Vortex Pulse Generation. *Opt Express* (2014) 22(21):26351–7. doi:10.1364/OE.22.026351
18. Bloch NV, Shemer K, Shapira A, Shiloh R, Juwiler I, Arie A. Twisting Light by Nonlinear Photonic Crystals. *Phys Rev Lett* (2012) 108(23):233902. doi:10.1103/PhysRevLett.108.233902
19. Liu D, Liu S, Mazur LM, Wang B, Lu P, Krolikowski W, et al. Smart Optically Induced Nonlinear Photonic Crystals for Frequency Conversion and Control. *Appl Phys Lett* (2020) 116(5):051104. doi:10.1063/1.5141420
20. Toyoda K, Takahashi F, Takizawa S, Tokizane Y, Miyamoto K, Morita R, et al. Transfer of Light Helicity to Nanostructures. *Phys Rev Lett* (2013) 110(14):143603. doi:10.1103/PhysRevLett.110.143603

21. Toyoda K, Miyamoto K, Aoki N, Morita R, Omatsu T. Using Optical Vortex to Control the Chirality of Twisted Metal Nanostructures. *Nano Lett* (2012) 12(7):3645–9. doi:10.1021/nl301347j
22. Minor CE, Cudney RS. Mirrorless Optical Parametric Oscillation in Bulk PPLN and PPLT: a Feasibility Study. *Appl Phys B* (2017) 123(1):38. doi:10.1007/s00340-016-6602-x
23. Harris SE. Proposed Backward Wave Oscillation in the Infrared. *Appl Phys Lett* (1966) 9(3):114–6. doi:10.1063/1.1754668
24. Strömqvist G, Pasiskevicius V, Canalias C, Montes C. Coherent Phase-Modulation Transfer in Counterpropagating Parametric Down-Conversion. *Phys Rev A* (2011) 84(2):023825. doi:10.1103/PhysRevA.84.023825
25. Strömqvist G, Pasiskevicius V, Canalias C, Aschieri P, Picozzi A, Montes C. Temporal Coherence in Mirrorless Optical Parametric Oscillators. *J Opt Soc Am B* (2012) 29(6):1194–202. doi:10.1364/JOSAB.29.001194
26. Shen YR. *The Principles of Nonlinear Optics*. New York: Wiley (1984). p. 138.
27. Canalias C, Pasiskevicius V. Mirrorless Optical Parametric Oscillator. *Nat Photon* (2007) 1(8):459–62. doi:10.1038/nphoton.2007.137
28. Ding YJ, Khurgin JB. Backward Optical Parametric Oscillators and Amplifiers. *IEEE J Quan Electron*. (1996) 32(9):1574–82. doi:10.1109/3.535361
29. Aadhi A, Samanta GK, Chaitanya Kumar S, Ebrahim-Zadeh M. Controlled Switching of Orbital Angular Momentum in an Optical Parametric Oscillator. *Optica* (2017) 4(3):349–55. doi:10.1364/OPTICA.4.000349
30. Abulikemu A, Yusufu T, Mamuti R, Araki S, Miyamoto K, Omatsu T. Octave-band Tunable Optical Vortex Parametric Oscillator. *Opt Express* (2016) 24(14):15204–11. doi:10.1364/OE.24.015204
31. Sharma V, Chaitanya Kumar S, Samanta GK, Ebrahim-Zadeh M. Orbital Angular Momentum Exchange in a Picosecond Optical Parametric Oscillator. *Opt Lett* (2018) 43(15):3606–9. doi:10.1364/OL.43.003606
32. Aadhi A, Samanta GK. High-power, High Repetition Rate, Tunable, Ultrafast Vortex Beam in the Near-Infrared. *J Opt* (2017) 20(1):01LT01. doi:10.1088/2040-8986/aa9a03

Conflict of Interest: The authors declare that the research was conducted in the absence of any commercial or financial relationships that could be construed as a potential conflict of interest.